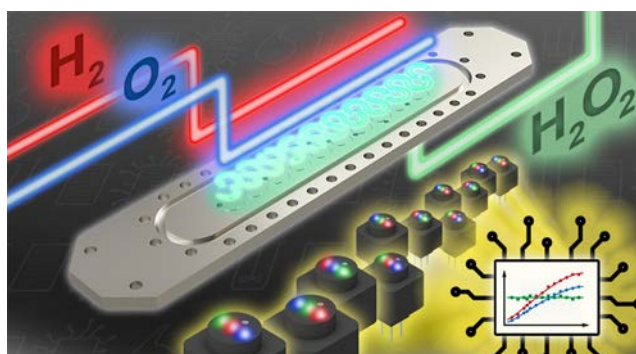


# In Situ Mapping of H<sub>2</sub>, O<sub>2</sub>, and H<sub>2</sub>O<sub>2</sub> in Microreactors: A Parallel, Selective Multianalyte Detection Method

Sebastian Urban, Benedikt J. Deschner, Laura L. Trinkies, Jochen Kieninger, Manfred Kraut, Roland Dittmeyer, Gerald A. Urban, and Andreas Weltin\*

**ABSTRACT:** Determining local concentrations of the analytes in state of the art microreactors is essential for the development of optimized and safe processes. However, the selective, parallel monitoring of all relevant reactants and products in a multianalyte environment is challenging. Electrochemical microsensors can provide unique information on the reaction kinetics and overall performance of the hydrogen peroxide synthesis process in microreactors, thanks to their high spatial and temporal resolution and their ability to measure in situ, in contrast to other techniques. We present a chronoamperometric approach which allows the selective detection of the dissolved gases hydrogen and oxygen and their reaction product hydrogen peroxide on the same platinum microelectrode in an aqueous electrolyte. The method enables us to obtain the concentration of each analyte using three specific potentials and to subtract interfering currents from the mixed signal. While hydrogen can be detected independently, no potentials can be found for a direct, selective measurement of oxygen and hydrogen peroxide. Instead, it was found that for combined signals, the individual contribution of all analytes superimposes linearly additive. We showed that the concentrations determined from the subtracted signals correlate very well with results obtained without interfering analytes present. For the first time, this approach allowed the mapping of the distribution of the analytes hydrogen, oxygen, and hydrogen peroxide inside a multiphase membrane microreactor, paving the way for online process control.

**KEYWORDS:** *electrochemical sensors, microreactor, hydrogen peroxide, hydrogen, oxygen, process monitoring*



Electrochemical sensors are an important subcategory of chemical sensors in which the rate of any given redox reaction taking place at an electrode is converted into an electrical signal. Ideally, a direct and linear correlation to the concentrations of the analytes involved in the electrode reactions can be obtained. If this correlation is known, for example, through prior calibration of the sensor, electrochemical sensors provide a comparatively inexpensive and simple method to monitor substances in a variety of different applications. They combine several preferable measurement characteristics: very exact measurements of even small concentration changes due to their high sensitivity and selectivity, defined zero points, linear detection over a wide range of analyte concentration, rapid sample to answer time, and high spatial and temporal resolution. At the same time, they enable the continuous acquisition of analyte concentrations in situ. This is rarely offered by other sensing methods, especially when considering additional factors, such as being competitive when it comes to instrumentation size, power, and cost requirements.<sup>1–7</sup> Electrochemical sensors are found in a variety of different commercialized applications like monitor

ing pH, dissolved oxygen, or concentrations of trace metals, carcinogens, and organic pollutants in the environment and in natural and ground water resources.<sup>1,8–12</sup> In recent years, their use in a wide range of additional research fields and commercial applications including, but not limited to, biosensors<sup>6,7</sup> and sensors for monitoring cell cultures by measuring metabolism markers was driven by a heavy focus on miniaturization and integration in microfluidic and clinical devices, for example, lab on a chip applications.<sup>5,13–16</sup> Concentrations of the dissolved gases hydrogen (H<sub>2</sub>) and oxygen (O<sub>2</sub>), as well as of hydrogen peroxide (H<sub>2</sub>O<sub>2</sub>), can be measured amperometrically by their direct oxidation (i.e., H<sub>2</sub> and H<sub>2</sub>O<sub>2</sub>) or reduction (i.e., O<sub>2</sub> and H<sub>2</sub>O<sub>2</sub>) on catalytically active noble metal electrodes, such as platinum. Measuring this

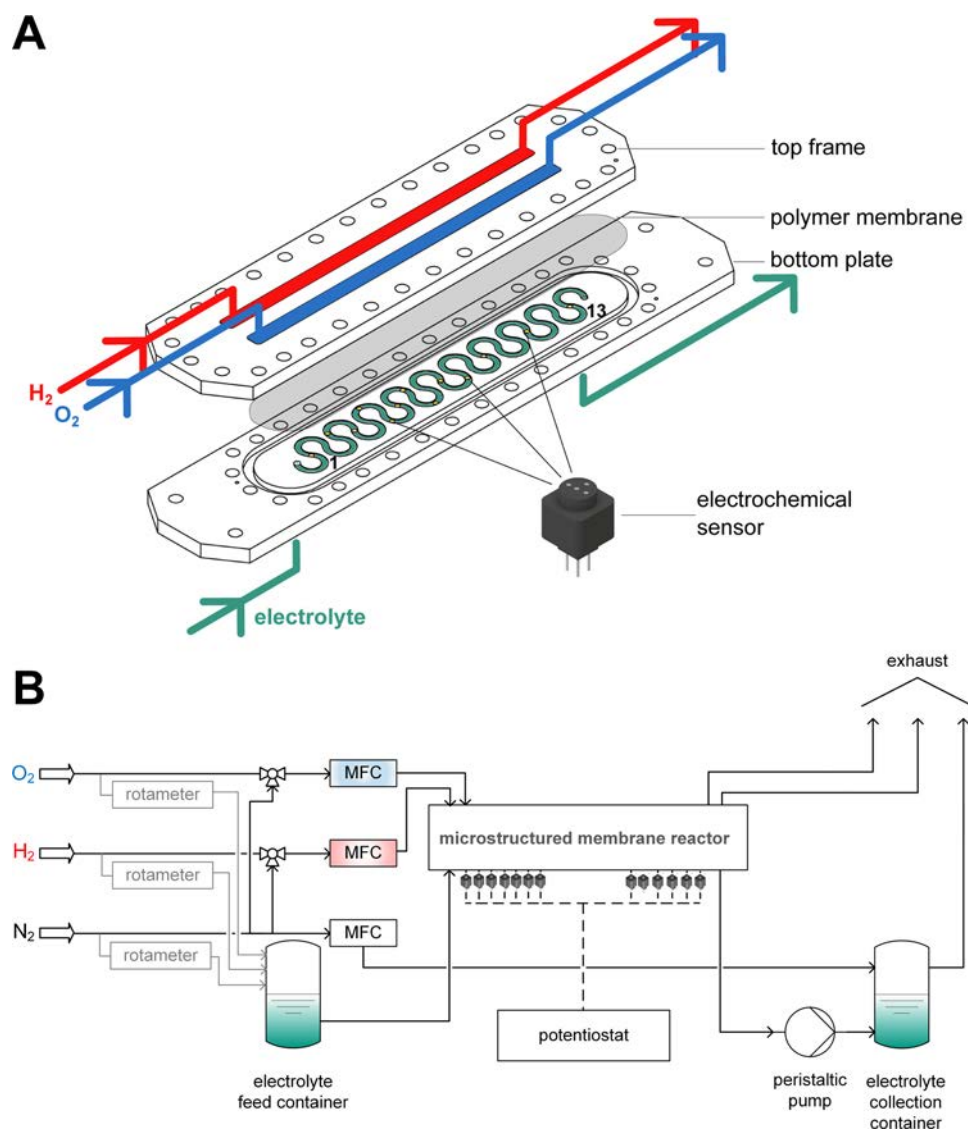


**Figure 1.** (A) Schematic depiction of the design and working principle of the direct synthesis membrane microreactor used for the measurement of  $\text{H}_2$ ,  $\text{O}_2$ , and  $\text{H}_2\text{O}_2$  with the chronoamperometric protocol. (B) Schematic of the whole measurement setup showing the reactor, gas/electrolyte supply, and the electrochemical sensor setup.

multianalyte system is however a challenging task considering overlapping oxidation and reduction potentials and therefore superimposed currents, finding electrode materials which are only sensitive to one of the dissolved molecules, and the lack of perm selective membranes because all molecules are very small and comparable in size.

An area where electrochemical sensors are rarely used to date is applications concerning micro process and reactor technology. While sensor integration and electrochemical sensing on the micro and nanoscale have been reported,<sup>17,18</sup> we aim at integration in stainless steel reactors at elevated pressure. In principle, the advantages offered by these sensors should be well suited for such applications as they offer the ability to continuously determine the reactant concentration in a fast, precise, and marker free way. Various reasons are responsible for the apparent lack of electrochemical sensors in microreactor applications. For one, it is very complex to miniaturize classical macroscopic sensors developed for process control for microfluidic applications and adapt them to the rather harsh process conditions. In particular, strongly

acidic or acidic solvent compositions as well as elevated operation pressures are predominately used in processes for manufacturing chemicals. These conditions typically result in very high analyte concentrations, largely exceeding the ones typically seen in the well established use cases of miniaturized electrochemical sensors.

The production of  $\text{H}_2\text{O}_2$  is an important example reaction that illustrates these harsh conditions.  $\text{H}_2\text{O}_2$  is a ubiquitous chemical commodity, often named a “key chemical” in the rising field of green and sustainable industrial chemistry.<sup>19</sup> Due to its excellent chemical properties as one of the most efficient oxidizing agents, it is used in a variety of very diverse applications. That includes not only the bleaching of pulp and paper, chemical synthesis processes but also a broad range of other sectors like the textile and cosmetic industries and wastewater treatment.<sup>20–23</sup> Despite its key role in the green chemistry industry, the production of  $\text{H}_2\text{O}_2$  still relies mainly on the centralized large scale synthesis by the very energy demanding anthraquinone process. It involves a complex multistage procedure consisting of hydrogenation and

subsequent oxidation and extraction steps.<sup>24</sup> Transportation to the point of use and the dilution from the high concentrations synthesized to the usually required 2–8 wt % considerably lowers its environmental and economic sustainability profile.<sup>25</sup> In recent years, this has led to an increased research interest to develop more sustainable synthesis methods, which target the onsite production of H<sub>2</sub>O<sub>2</sub> on a small and intermediate scale. The two most promising approaches for a simpler and green production of H<sub>2</sub>O<sub>2</sub> are the electrochemical synthesis by means of the oxygen reduction reaction using metal free carbon catalysts<sup>20,28–28</sup> and the heterogeneously catalyzed direct synthesis of H<sub>2</sub>O<sub>2</sub> from H<sub>2</sub> and O<sub>2</sub> using noble metal catalysts.<sup>29–33</sup> The latter is especially interesting considering recent advancements in synthesis reactor designs toward micro structuring of the channels for increased mass transfer capabilities, combined with intensification methods like using membranes for dosing the reactant gases into the liquid phase.<sup>31,32</sup> However, for process optimization and a safe process performance, the concentrations of reactants (H<sub>2</sub> and O<sub>2</sub>) and product (H<sub>2</sub>O<sub>2</sub>) should be constantly monitored, ideally in situ, that is, inside the microreactor during the synthesis process. Different detection methods are available for determining the concentrations of analytes involved in the synthesis, for example, for H<sub>2</sub>O<sub>2</sub>, such as titration using permanganate,<sup>34</sup> fluorescence,<sup>35</sup> chemiluminescence,<sup>36,37</sup> and spectroscopy.<sup>38</sup> However, they are not easy to integrate into microreactor layouts without disturbing the flow or the chemistry. Therefore, they only allow measurements at the outlet of the reactor. Moreover, most of these techniques require additional reactants incompatible with the synthesis process.

In previous works, we presented an electrochemical sensor system that was successfully integrated into a microreactor.<sup>39,40</sup> These sensors allowed the amperometric detection of elevated concentrations of the single analytes, that is, dissolved process gases H<sub>2</sub> (40 mM), O<sub>2</sub> (50 mM), and their reaction product H<sub>2</sub>O<sub>2</sub> (20 mM) with linear current signal to concentration relation at high pressures up to 70 bar.<sup>39</sup> However, to be able to adequately control the synthesis, one needs to ideally measure all three reactants at the same time.

Therefore, in this work, we propose a chronoamperometric protocol which allows the parallel, selective electrochemical determination of H<sub>2</sub>, O<sub>2</sub>, and H<sub>2</sub>O<sub>2</sub> on the same platinum working electrode. By choosing specific potentials for each step in the chronoamperometric protocol, we can minimize the interference of two of the reactants and are able to selectively determine the concentration of the third. This allows the subsequent subtraction of the thus known concentration of this analyte for the current signals for the other two. Experiments conducted inside the microreactor confirm the validity of this novel approach.

## METHODS

**Synthesis Microreactor and Measurement Setup.** The reactor used in our experiments was originally designed for the continuous direct synthesis of H<sub>2</sub>O<sub>2</sub>.<sup>32</sup> Therefore, the two gaseous reactants H<sub>2</sub> and O<sub>2</sub> are led in individual gas compartments over a curvilinear reaction channel, which is separated from the gases by a composite polymer membrane [polydimethylsiloxane (PDMS) flat sheet membrane, PERVATECH, The Netherlands]. The detailed concept has been presented before,<sup>31,32</sup> and a schematic overview of the reactor layout is given in Figure 1A. The dense polymer membrane is made of a PDMS film, deposited onto a porous polyimide intermediate layer and a porous polyethylene terephthalate

support layer. A frame holds the membrane in place on top of the curvilinear microchannel and separates the gas compartments measuring 10 mm in width. The curvilinear microchannel is 0.77 m long and features a rectangular cross section (4 mm width × 0.5 mm height). The channel design allows the liquid electrolyte to be alternately resaturated with the two reacting gases from the top. The bottom of the curvilinear channel has openings for up to 13 sensor plugs used in the electrochemical measurements.

The setup in operation for the experiments can be seen in Figure 1B. Mass flow controllers (EL FLOW, Bronkhorst, The Netherlands) fed the gaseous components to be detected, H<sub>2</sub> and O<sub>2</sub>, as well as gaseous nitrogen (N<sub>2</sub>) into the reactor via stainless steel tubing. N<sub>2</sub> served as optional diluent of the main gas components and was also used to flush the setup between and after the experiments to increase the safety of the system. In the experiments presented, the gas flow rates were set to 150 mL/min for each gas channel at ambient pressure. For the measurements with a presaturated solvent, additional variable area flow meters dosed the corresponding saturating gas via tubes into the electrolyte container. With this arrangement, the electrolyte feed container can be saturated with any combination of these gases at room temperature. Either two of the three connected pure gases flow through the two gas compartments of the reactor or, using a tube fitting, both gas zones can also be flown through with the same gas composition. The liquid electrolyte itself was aspirated through the liquid side of the reactor by a peristaltic pump (MINIPULS 3, Gilson, USA) at flow rates of 0.6, 1.2, and 2.3 mL/min, respectively. The base solvent was composed of 0.15 mM sulfuric acid (H<sub>2</sub>SO<sub>4</sub>) (diluted from H<sub>2</sub>SO<sub>4</sub> 0.1 mol/L in aqueous solution, VWR Chemicals, France) and 4 mM sodium bromide (NaBr) (extra pure, Merck, Germany) in water (Milli Q purified), resulting in a pH of 3.5. For measurements involving H<sub>2</sub>O<sub>2</sub>, electrolyte solutions with 0.5, 1, and 2 mM H<sub>2</sub>O<sub>2</sub> were prepared from a 30% H<sub>2</sub>O<sub>2</sub> stock solution (Perhydrol p.a. EMSURE ISO, Merck, Germany).

All experiments were conducted under ambient conditions (room temperature and atmospheric pressure). The stainless steel parts of the setup had been passivated with a HNO<sub>3</sub> solution prior to use.<sup>41</sup> We note that H<sub>2</sub>/O<sub>2</sub> gas mixtures are explosive in a wide range (4–96 vol %) at atmospheric pressure.<sup>42</sup> Therefore, the electrolyte collection container was permanently flushed with N<sub>2</sub> in all experiments to ensure that the hydrogen concentration remains below the lower explosive limit. Moreover, the reactor was also flushed with pure N<sub>2</sub> between and after the experiments. This is crucial to exclude possible explosive gas mixtures within the reactor caused by the different gas compositions used in the course of the experiments.

**Sensor Device Fabrication.** The electrochemical sensors consist of three, circular shaped, platinum disk electrodes with a diameter of 300 μm, used as working and counter electrodes. Additionally, one 500 μm silver/silver bromide (Ag/AgBr) electrode is employed on the same sensor device as the pseudo reference electrode utilizing the fixed amount of bromide ions present in the electrolyte. The Pt and Ag electrode wires (99.99%, chemPUR, Germany) were cut into length and soldered into a four pin 1.27 mm pitch IC connector. The as prepared wires were subsequently fixed into a polytetrafluoroethylene (TECAFLON PTFE, Ensinger, Germany) casting mold, encapsulated into a two component epoxy housing (Loctite Stycast 2057 and Loctite Cat 9, Henkel, Germany) and cured for 6 h at 60 °C. A more detailed report on the sensor fabrication was published previously.<sup>40</sup> After complete hardening of the sensor plug housing, the electrodes were ground to obtain a perfect circular shape and polished using alumina (Al<sub>2</sub>O<sub>3</sub>) powder of three different grain sizes (Alpha Alumina Powder 1.0, 0.3, and 0.05 μm, CH Instruments, USA) with intermediate rinsing steps using deionized water. The Ag/AgBr pseudo reference was then deposited on the silver electrode by immersion into 0.1 mM potassium bromide (KBr p.a., Merck, Germany) solution using an anodic bromination method, as described before,<sup>39</sup> and again rinsing in deionized water for 1 min. In a final step, a diffusion limiting barrier with a thickness of approximately 35 μm was applied to all four electrodes using a poly(hydroxyethyl methacrylate) based hydrogel, as described previously.<sup>39,43</sup>

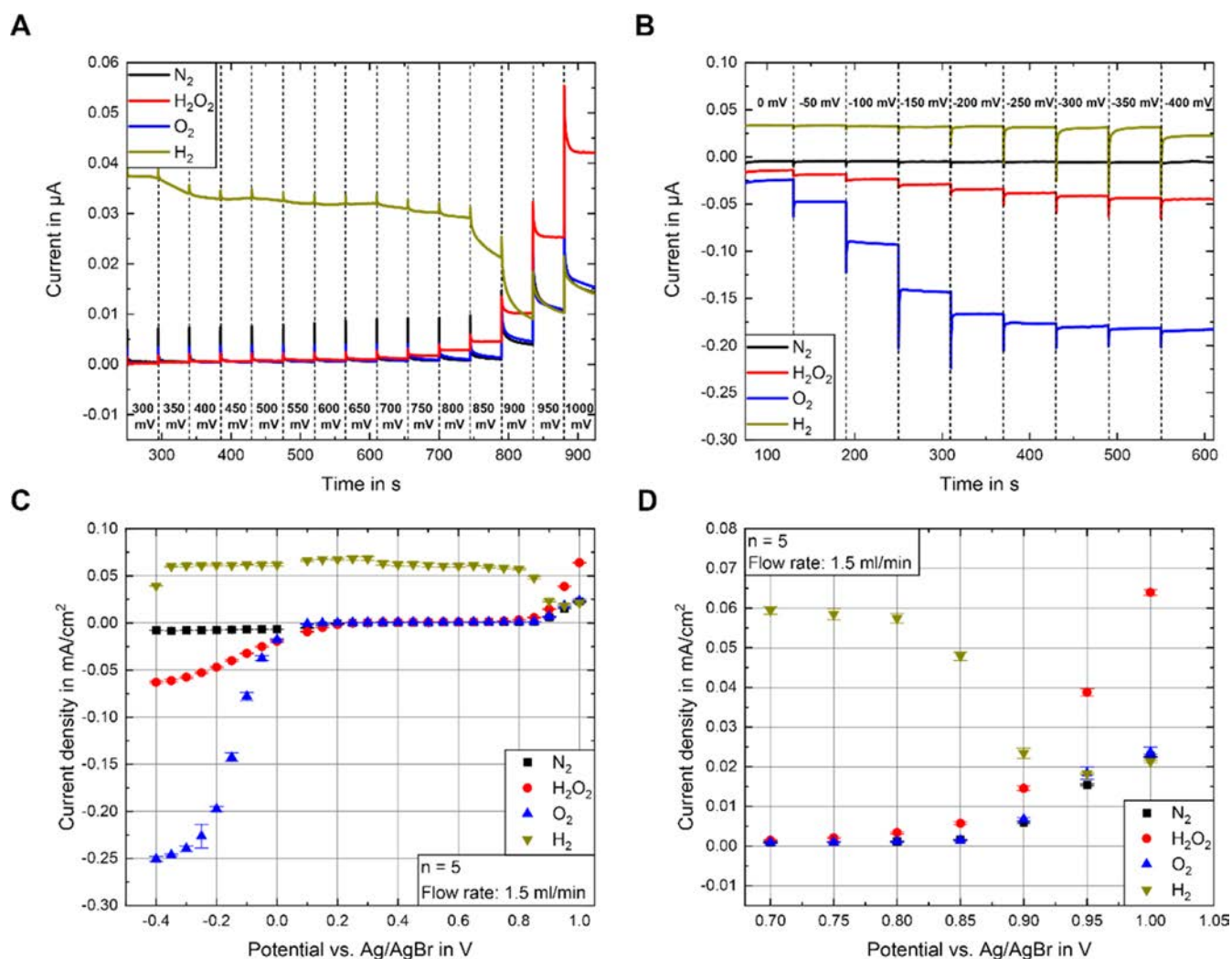


**Figure 2.** (A,B) Transient signals at applied positive (A) and negative (B) potentials for saturated concentrations of  $\text{O}_2$  and  $\text{H}_2$  and 1 mM  $\text{H}_2\text{O}_2$  in an electrolyte containing 0.15 mM  $\text{H}_2\text{SO}_4$  and 4 mM NaBr. Additionally, an  $\text{N}_2$  flushed electrolyte provided an analyte free background signal. (C) Arithmetic mean values of the current densities over potential for the combined chronoamperometric measurements (see A,B).  $\text{H}_2$  oxidation can be observed across almost the complete range.  $\text{H}_2\text{O}_2$  is oxidized above 0.8 V and reduced below 0.2 V.  $\text{O}_2$  is reduced below 0.1 V. (D) Enlargement of the potential region from 0.7 to 1 V vs Ag/AgBr, where  $\text{H}_2$  sensitivity decreases and  $\text{H}_2\text{O}_2$  sensitivity increases.

**Electrochemical Sensor Protocol.** The intention was to develop a chronoamperometric sensor protocol, which allows the selective measurement of several oxidizable and reducible species, on a single, except for a diffusion limiting barrier, unmodified platinum electrode. In this particular application case, these species are the dissolved synthesis reaction analytes  $\text{H}_2$ ,  $\text{O}_2$ , and  $\text{H}_2\text{O}_2$ . The main challenge arrives from concurrent redox processes, overlapping over a wide range of anodic and cathodic potentials. It is therefore crucial to determine measurement potentials which allow for a selective signal for any given analyte, optimally completely free of any influence of other chemical species present in the same electrolyte. The boundaries for choosing appropriate measurement potentials on a platinum electrode are furthermore limited by the water window, which lies approximately between  $-0.03$  and  $1.48$  V versus the reversible hydrogen electrode (RHE), beyond which  $\text{H}_2$  and  $\text{O}_2$  evolution would ensue in the cathodic and anodic region, respectively, and should therefore be avoided.

For this particular combination of analytes, it is not possible to determine their concentrations from three independent measurement signals. Instead, the chronoamperometric protocol is used to determine the concentration of one of the analytes by choosing an appropriate potential and then calculating the concentration of the other two from the mixed signals measured at a different potential

step in the chronoamperometric protocol. For the successful implementation of such an elaborate sensing technique, certain requirements have to be fulfilled regarding the interaction of the analytes and their corresponding mixed signals acquired by the sensing protocol. This will be discussed in Results and Discussion.

All electrochemical measurements were carried out using chronoamperometric protocols with the sensor plugs, as described in Sensor Device Fabrication, installed into the microreactor setup. The experiments were performed with a four channel MultiEmStat3 potentiostat (Palsens BV, The Netherlands). If not stated otherwise, potentials are reported and applied versus the on plug Ag/AgBr reference electrode in 4 mM NaBr and 0.15 mM  $\text{H}_2\text{SO}_4$  electrolyte (+6 mV vs saturated Ag/AgCl reference).

## RESULTS AND DISCUSSION

### Determination of Selective Measurement Potentials.

Chronoamperometric measurements were performed inside the microreactor setup to determine the optimal measurement for each of the three analytes. Two different protocols were run, one for anodic potentials and one for cathodic potentials. Each protocol was preceded by five consecutive pretreatment cycles of the alternating potentials of 0.9 and  $-0.3$  V versus

Ag/AgBr to guarantee a reproducible and clean state of the platinum electrode. Afterward, increasing (0.1 to 1 V vs Ag/AgBr) and decreasing (0 to  $-0.4$  V vs Ag/AgBr) potentials were applied in 50 mV intervals, each for 45 and 60 s, respectively. Figure 2A,B shows the transient current responses obtained inside the microreactor for the chronoamperometric measurements in the anodic and primarily cathodic regions, respectively, for electrolytes flushed with  $H_2$  and  $O_2$  and spiked with 1 mM  $H_2O_2$ . Additionally, the protocol was also run with the electrolyte flushed with  $N_2$  to obtain a zero analyte reference signal.

As shown in Figure 2C, the arithmetic mean values of the current densities for five measurements with the chronoamperometric protocol for each of the analytes were plotted for all applied potentials. The measurement for the  $H_2$  saturated electrolyte shows a relatively stable oxidation current density over the whole potential range. Approaching the most negative potential of  $-0.4$  V versus Ag/AgBr (0.03 V vs RHE), a lower current density was observed. This can be explained by the potential value approaching the theoretical thermodynamic onset potential for the hydrogen oxidation reaction (HOR) of 0 V versus RHE. An even stronger decline in signal strength can be observed for anodic potentials above 0.7 V versus Ag/AgBr, which results in an almost complete inhibition of the HOR for potentials above 0.9 V versus Ag/AgBr, as seen in Figure 2D, due to the formation of platinum oxide (PtO) at the electrode surface.<sup>44,45</sup> This is further evidenced by the fact that the onset of  $H_2O_2$  oxidation coincides with the decrease of the HOR signal. The oxidation of  $H_2O_2$  requires the presence of PtO.<sup>46</sup> The comparatively high anodic potentials necessary to form PtO can be explained by the presence of bromide ions in the electrolyte, which block the necessary binding sites for the formation of PtO, until the bromide is oxidized at potentials above 0.8 V, as described in the literature.<sup>39,47,48</sup> This oxidation process of bromide to bromine also adds a background signal to the measurement, as seen in Figure 2D.

$O_2$  cannot be detected at potentials where  $H_2O_2$  is oxidized.  $O_2$  can only be reduced at bare Pt, whereas  $H_2O_2$  can only be oxidized on PtO. PtO is formed from water and is independent from the amount of dissolved molecular  $O_2$  in the solution.  $O_2$  can be reduced to water in a mechanism yielding four electrons per oxygen molecule. Figure 2B shows the increasing reduction currents for  $O_2$  with increasingly negative overpotentials, reaching diffusion limitation at around  $-0.3$  V. For all possible reduction potentials, the  $O_2$  signal overlaps with the reduction of  $H_2O_2$  and the oxidation of  $H_2$ . That makes it impossible to directly determine the  $O_2$  concentration in an electrolyte with all three analytes present. The concentrations of the other two analytes,  $H_2$  and  $H_2O_2$ , can be independently determined by choosing the correct oxidation potentials (0.35 to 0.65 V for  $H_2$  and  $\geq 0.95$  V for  $H_2O_2$ ). Thus, the  $O_2$  concentration can be determined by the subtraction of the redox signals for the known concentration of these two interfering analytes from the overall signal at the  $O_2$  detection potential. This only works when assuming that the redox processes at the electrode are independent of each other and the resulting currents are therefore additive. This usually holds true as long as the redox processes occurring at the electrode do not produce an intermediate or product which diffuses away from the electrode and reacts with one of the other analytes, or the diffusion constants of the involved analytes differ greatly from each other.<sup>49–51</sup> In theory, both of these cases should not apply for the combination of  $H_2$ ,  $O_2$ , and  $H_2O_2$  but the linear,

additive behavior needs to be thoroughly examined in order to use the proposed subtraction method.

**Characterization of the  $H_2O_2/H_2$  Interference.** Chronoamperometric measurements were performed to examine the interaction of the measured currents of  $H_2$  and  $H_2O_2$  when both are present in the same electrolyte. The chronoamperometric protocol consisted of three steps: an anodic potential of 1.00 V to oxidize the platinum electrode surface, which is needed in the following step to oxidize the  $H_2O_2$ . The second step varied between 0.80 and 0.95 V. A final third step is applied by switching to a cathodic potential of  $-0.3$  V. Each potential was applied for 5 s. The protocol was then used to measure calibration curves for dissolved  $H_2$  with different amounts of  $H_2O_2$  applied to the same electrolyte.

For anodic potentials, measurements showed that even though values of above 0.7 V increasingly inhibit the HOR, a background  $H_2$  oxidation signal cannot completely be eliminated. Figure 3A shows this exemplified for 0.95 V, the highest anodic potential used, which still shows a linear

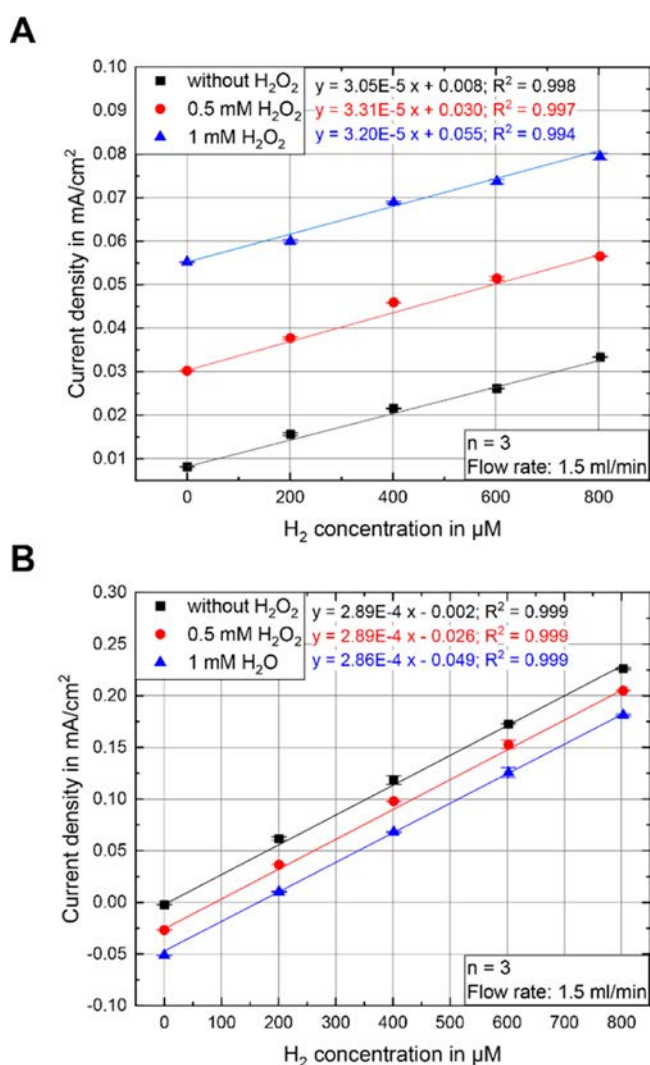


**Figure 3.** (A) Anodic  $H_2$  calibration curves at a potential of 0.95 V vs Ag/AgBr show linear additive relationship with increasing  $H_2O_2$  concentrations. (B)  $H_2$  calibration curves at a potential of  $-0.3$  V show a linear, negatively superimposed current on the  $H_2$  oxidation signal with increasing  $H_2O_2$  concentrations due to its simultaneous reduction.

increase of the measurement signal with increasing  $H_2$  concentration. Adding different  $H_2O_2$  concentrations does not change the slope of the  $H_2$  concentration curves and instead adds on linearly on top of the signal. The same behavior can be observed, when plotting the measurement data for the changing  $H_2O_2$  concentration (not shown). The presence of  $H_2$  does not change the slope for any measured  $H_2O_2$  concentration but superimposes a background signal on top which changes linearly with the concentration. This allows a simple elimination of the  $H_2$  background by determining the concentration at a lower, selective potential and subtracting the corresponding current for this potential.

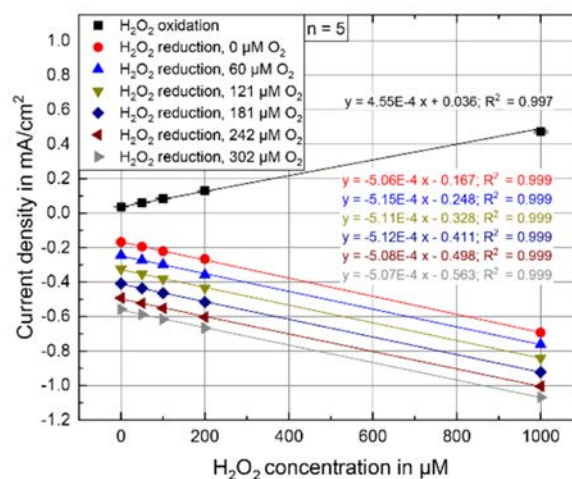
Applying the cathodic potential of  $-0.3$  V results in a similar behavior. As seen in Figure 3B, the oxidation currents of  $H_2$  still increase linearly with increased dissolved gas concentration. The slope of the concentration curves is about 1 order of magnitude higher than for the anodic potential of  $0.95$  V since no inhibiting PtO is formed at these low potentials. Adding higher quantities of  $H_2O_2$  again superimposes a background signal which behaves linearly with concentration. This time, though, it subtracts from the signal with no  $H_2O_2$  present since  $H_2O_2$  is reduced at  $-0.3$  V. Again, this allows an easy determination of either concentration by subtracting the signal of the other analyte, if the concentration of the analyte is known or can be determined at a different potential.

**Characterization of the  $H_2O_2/O_2$  Interference.** To analyze whether the interaction between  $H_2O_2$  and  $O_2$  behaves similar to the interaction between  $H_2O_2$  and  $H_2$ , calibration curves were recorded for the anodic and cathodic detection of  $H_2O_2$ . Preliminary results have been reported previously.<sup>52</sup> Calibration curves were obtained with the same chronoamperometric measurement protocol as mentioned in Characterization of the  $H_2O_2/H_2$  Interference and repeated five times for each measurement. Each calibration was then repeated for different concentrations of dissolved  $O_2$  in the electrolyte. In contrast to  $H_2$ , dissolved  $O_2$  is not expected to influence the  $H_2O_2$  signal at high potentials from  $0.8$  to  $0.95$  V<sup>53</sup> as it is neither involved in the formation of PtO nor reducible on PtO. Accordingly, no difference in either absolute values or in slope could be detected when recording  $H_2O_2$  calibration curves with or without  $O_2$  being present in the electrolyte. One exemplary anodic  $H_2O_2$  calibration curve is shown in Figure 4A.

Also shown in Figure 4A are the calibration curves for  $H_2O_2$  at the reduction potential of  $-0.3$  V. It can be seen that the sensitivity does not change with increasing concentrations of  $O_2$ . Instead, the measured absolute currents increase in a linear manner relative to the change in  $O_2$  concentrations. This allows the subsequent subtraction of the  $H_2O_2$  reduction current from the  $O_2$  reduction current by using the  $H_2O_2$  oxidation signal (where  $O_2$  has no influence), determined in the first step of the chronoamperometric protocol, and calculating the corresponding superimposed  $H_2O_2$  reduction signal.

This behavior was verified for cathodic  $O_2$  measurement by conducting  $O_2$  calibrations at  $-0.3$  V with different concentrations of  $H_2O_2$  present in the solution. These measurements were repeated five times each. Figure 4B shows the results for the calibration. They support the former results as the increasing  $H_2O_2$  concentration does not affect the slope of the curves and only increases the measurement signal in a linear additive manner, allowing the use of the proposed subtraction method to determine the  $O_2$  concen-

A



B

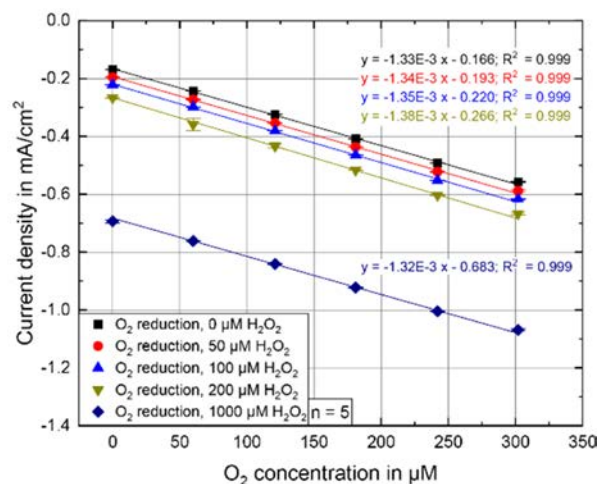


**Figure 4.** (A) Cathodic  $H_2O_2$  calibration curves performed at a potential of  $-0.3$  V and exemplary anodic  $H_2O_2$  calibration performed at  $0.8$  V. The increasing concentrations of  $O_2$  superimpose in a linear additive manner on the cathodic signal. (B)  $O_2$  calibrations performed at  $-0.3$  V. Increasing concentrations of  $H_2O_2$  do not change the sensitivity but superimpose in a linear additive manner on the  $O_2$  signal.

tration while the interfering reactant  $H_2O_2$  is present in the electrolyte.

**Chronoamperometric Measurement Protocol.** From the examined interactions of the analytes  $H_2$ ,  $O_2$ , and  $H_2O_2$  in the prior sections, it is possible to deduce a chronoamperometric protocol which allows the determination of each analyte's concentration with the very same working electrode. The process itself only requires a prior calibration of all involved analytes for the different measurement potentials used in the measurement protocol.

Figure 5 shows the complete chronoamperometric protocol and corresponding current signal response for each analyte involved, compared to a  $N_2$  flushed, analyte free electrolyte. It consists of four different potential steps: three primarily anodic and one primarily cathodic in descending order for one measurement cycle. Each applied potential is marked at the top of the corresponding range. In a first preconditioning step at a potential of  $1$  V, the bare platinum is oxidized to PtO. This step is not crucial but increases the reproducibility of the

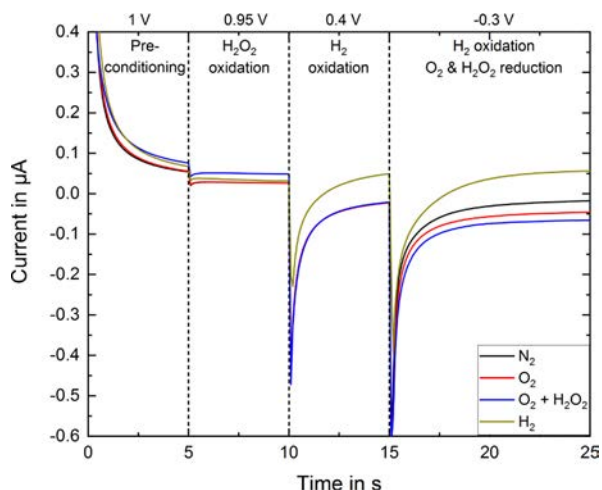


**Figure 5.** Current response of one scan of the developed multistep chronoamperometric sensor protocol for different analytes present in the electrolyte. In four chronoamperometric steps, four different potentials are set:  $E_{\text{PtO}} = 1 \text{ V}$  for PtO formation,  $E_{\text{H}_2\text{O}_2} = 0.95 \text{ V}$  for anodic sensing of  $\text{H}_2\text{O}_2$ ,  $E_{\text{H}_2} = 0.4 \text{ V}$  for anodic sensing of  $\text{H}_2$ , and  $E_{\text{O}_2} = -0.3 \text{ V}$  for cathodic sensing of  $\text{O}_2$  after subtracting the calculated signals of  $\text{H}_2$  and  $\text{H}_2\text{O}_2$ .

following measurements. It is followed by a slightly lower anodic potential  $0.95 \text{ V}$  for the oxidation of  $\text{H}_2\text{O}_2$ . This potential is chosen rather high to minimize the influence of a simultaneously occurring  $\text{H}_2$  oxidation current. Though it cannot be completely eliminated, its addition to the overall signal strength, even for high  $\text{H}_2$  concentrations (saturation concentration at ambient pressure is  $806 \mu\text{M}$ ), is quite small (as seen in Figure 5) and behaves linearly additive (as shown in Characterization of the  $\text{H}_2\text{O}_2/\text{H}_2$  Interference). The third step is another anodic step of  $0.4 \text{ V}$  and the most important step for the overall sensor protocol and subtraction method. This potential allows for a completely independent determination of the dissolved  $\text{H}_2$  concentration by oxidation as neither  $\text{O}_2$  nor  $\text{H}_2\text{O}_2$  is oxidizable or reducible in this region. Being able to determine, one of the three analytes independently allows for the eventual determination of the other two. The last step of the protocol switches to the primarily cathodic potential of  $-0.3 \text{ V}$ . As exhibited by Figure 5, all three analytes are either oxidized ( $\text{H}_2$ ) or reduced ( $\text{O}_2$  and  $\text{H}_2\text{O}_2$ ) in this region. A determination of the individual current contribution of each analyte is possible with the following proposed subtraction method.

With the known concentration of  $\text{H}_2$ , determined independently at  $0.4 \text{ V}$ , it is possible to calculate its expected current contribution at the other potentials, that is,  $0.95$  and  $-0.3 \text{ V}$ . That requires an independent calibration of all three analytes at the three measurement potentials. Ideally, these calibrations are performed with the exact same chronoamperometric protocol used for the actual application. The known  $\text{H}_2$  concentration allows calculating the current contribution of  $\text{H}_2$  for the other two applied potentials, by applying it to their respective calibration equations. When subtracted from the measurement signal at the potential of  $0.95 \text{ V}$ , one obtains the oxidation current for  $\text{H}_2\text{O}_2$ . This enables the determination of the  $\text{H}_2\text{O}_2$  concentration with the help of the respective calibration curve. With two of the analyte concentrations known, the same method can be applied to the measurement signal obtained at  $-0.3 \text{ V}$  to calculate the  $\text{O}_2$  concentration. A

concise overview of the involved steps is given in Table 1. Although, the algorithm is rather complex, it is easy to adapt into an automatic analysis process because it only needs processing of the one single measurement signal.

**Table 1. Step by Step Description for Obtaining the Concentrations of the Analytes  $\text{H}_2$ ,  $\text{O}_2$ , and  $\text{H}_2\text{O}_2$  with the Help of the Proposed Chronoamperometric Protocol**

step #	description
1	independent calibration of $\text{H}_2$ , $\text{O}_2$ , and $\text{H}_2\text{O}_2$ at all measurement potentials
2	measurement of $\text{H}_2$ at the potential of $0.4 \text{ V}$
3	calculation of the corresponding current contribution of $\text{H}_2$ for the signal at $0.95 \text{ V}$ from the calibration curve
4	subtraction of the $\text{H}_2$ current contribution from the signal yields $\text{H}_2\text{O}_2$ current contribution and allows determination of $\text{H}_2\text{O}_2$ from the calibration curve
5	calculation and subtraction of current contribution of $\text{H}_2$ and $\text{H}_2\text{O}_2$ from signal at $-0.3 \text{ V}$
6	obtaining $\text{O}_2$ concentration from resulting current with the help of the corresponding calibration curve

**In Situ Characterization of the Sensor Protocol in the Membrane Microreactor.** The developed sensor protocol was tested and characterized in the synthesis reactor setup, as described in Sensor Device Fabrication. The microreactor setup allows for measurement with concurrent, saturated concentrations of the dissolved gases  $\text{H}_2$  and  $\text{O}_2$  in the same electrolyte inside a safe reactor environment. In contrast, presaturating an undiluted gas mixture of  $\text{H}_2$  and  $\text{O}_2$  in a general purpose electrochemical cell would bear considerable safety risks. Furthermore, the reactor constitutes a suitable in situ test case for the developed sensor protocol as all three analytes can be combined in a safe manner and the local dissolved gas concentration pattern can be determined for the first time over the whole channel length. A total of 13 different sensor positions are available in the reactor at the bottom of the curvilinear channel. The used four channel potentiostat only allows for the simultaneous measurement of four sensor positions. Therefore, each experiment was performed at least four times, each time with a different sensor distribution, to be able to completely map the analyte concentration for all 13 sensor positions inside the reactor. For all of these four measurements, the same four sensor plugs were used. Sensor positions which were not used for the performed measurement were equipped with dummy plugs to seal the reactor. The measurements presented here were performed without any catalyst present in the setup as the focus was to test and characterize the sensor protocol feasibility, not the synthesis process. All sensors were calibrated for all three analytes independently in the reactor, with the same chronoamperometric protocols as used for the measurement.

**Simultaneous Detection of  $\text{H}_2$  and  $\text{O}_2$  Entering the Microreactor.** Measurements were performed in which both reactant gases,  $\text{H}_2$  and  $\text{O}_2$ , were simultaneously fed to the reactor in their corresponding individual gas compartments over the curvilinear reaction channel, while the electrolyte feed container was flushed with pure  $\text{N}_2$ . The experiment was executed for three different volumetric flow rates of the liquid electrolyte ( $0.6$ ,  $1.2$ , and  $2.3 \text{ mL/min}$ ), resulting in laminar flow. With the help of the chronoamperometric protocol, the  $\text{H}_2$  concentration was measured at each of the 13 sensor positions, while the  $\text{O}_2$  concentration was determined by the

steps described in Table 1. Figure 6A,B shows the measured concentration patterns of H<sub>2</sub> and O<sub>2</sub>, respectively, over the

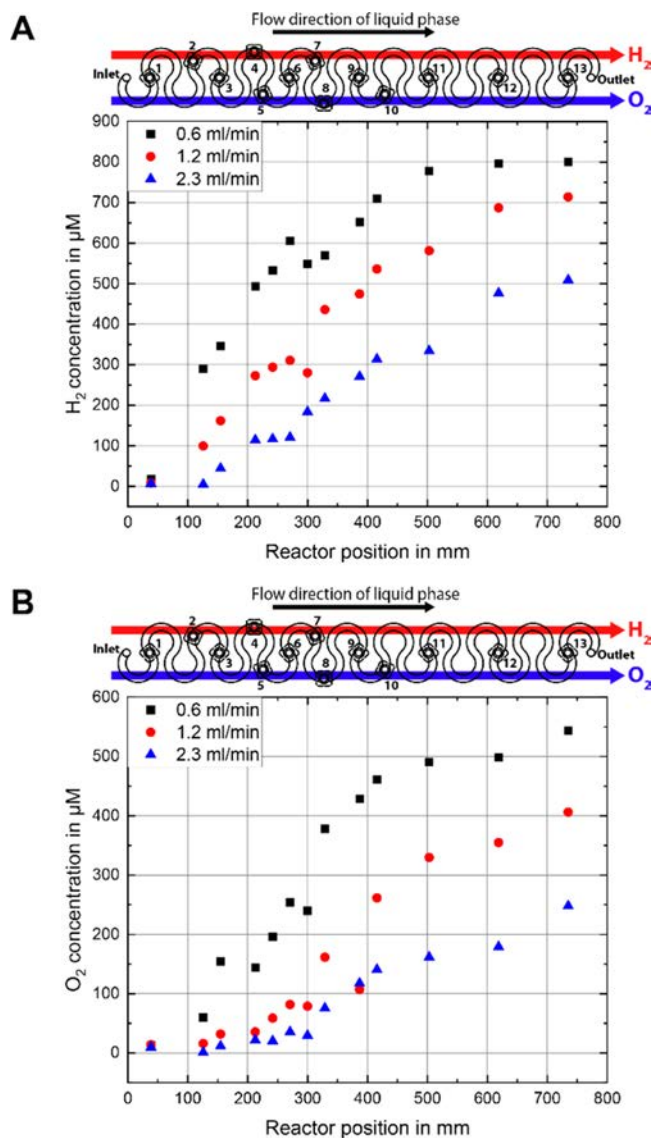


**Figure 6.** (A) H<sub>2</sub> concentrations along the membrane microreactor during the simultaneous detection of dissolved H<sub>2</sub> and O<sub>2</sub> for three different electrolyte flow rates. (B) O<sub>2</sub> concentrations along the membrane microreactor during the simultaneous detection of dissolved H<sub>2</sub> and O<sub>2</sub> for three different electrolyte flow rates.

length of the curvilinear reaction channel. The sensor positioning inside the microchannel is schematically shown above the graphs with the corresponding pathway of the gas channels. The width of the gas channels in the schematic is not to scale.

As expected, both dissolved gas concentrations increase along the reactor as the flowing liquid progressively gets in contact with more membrane area for transferring H<sub>2</sub> and O<sub>2</sub>. The sensors reveal that the lower the volumetric flow rate of the electrolyte, the higher the dissolved gas concentrations. That is because the residence time of the electrolyte increases and therefore its exposure time to the gases. In detail, the dissolved H<sub>2</sub> concentration linearly rises until ca. 75 to 80% of its thermodynamic saturation concentration (806 µM) is reached, followed by a pronounced flattened increase. In

contrast, O<sub>2</sub> only shows a near linear increase for the lowest flow rate of 0.6 mL/min. For higher flow rates, the onset of a significant change of O<sub>2</sub> concentration appears to be delayed, resulting in the curveform more resembling a sigmoid function. This flattening of the dissolved gas concentration can be explained by a steadily decreasing driving force of the transmembrane flux: with increasing distance from the inlet, more and more H<sub>2</sub> and O<sub>2</sub> are already present in the liquid phase, lowering the concentration gradient between both phases. Furthermore, the liquid phase O<sub>2</sub> concentration is smaller for all applied flow rates in comparison to the corresponding H<sub>2</sub> concentrations. This is in good agreement with the diffusion coefficients for both dissolved gases in pure water, with H<sub>2</sub> diffusivity ( $4.58 \times 10^{-9} \text{ m}^2 \text{ s}^{-1}$  at 20 °C) being approximately twice as fast compared to O<sub>2</sub> ( $2.01 \times 10^{-9} \text{ m}^2 \text{ s}^{-1}$  at 20 °C).<sup>54</sup> In addition to the overall sigmoidal pattern, the individual position of the sensor in relation to each gas channel also needs to be considered. Since the polymer membrane is not permselective, a fraction of dissolved H<sub>2</sub> escapes to the O<sub>2</sub> gas channel and vice versa. Thus, the dissolved concentration of the chemical species in the liquid phase, which is not present in the gas phase in the respective reactor section, locally decreases to a certain extent. This effect was observed in the O<sub>2</sub> curves, for example, at position 4, 7, and 12, where the measurement is performed in, or shortly after the H<sub>2</sub> gas zone.

**Simultaneous Detection of H<sub>2</sub> and O<sub>2</sub> at Different H<sub>2</sub>O<sub>2</sub> Levels.** The experiments were repeated with H<sub>2</sub>O<sub>2</sub> present in the electrolyte. Three different concentration levels of H<sub>2</sub>O<sub>2</sub> (0.5, 1, and 2 mM) were adjusted in the electrolyte reservoir before starting the measurement. Figure 7A shows the detected H<sub>2</sub>O<sub>2</sub> concentration in the reactor after subtracting the calculated H<sub>2</sub> signal from the mixed current according to the steps listed in Table 1. The measured concentrations fit very well with the preapplied concentrations. Averaging the values of all positions, the highest error of around 5.2% is found at 0.5 mM concentration. As shown in Figure 7B, the presence of H<sub>2</sub>O<sub>2</sub> does not influence the measurement of the H<sub>2</sub> concentration as all measurements with different H<sub>2</sub>O<sub>2</sub> concentrations fit well to measurements without H<sub>2</sub>O<sub>2</sub>. This confirms again that, at the chosen potential of 0.4 V, H<sub>2</sub> can be measured independent of the other analytes. Since both H<sub>2</sub> and H<sub>2</sub>O<sub>2</sub> concentrations obtained with the chronoamperometric protocol fit the expected results, they can be used to subsequently calculate and subtract their corresponding current contribution at the cathodic potential of -0.3 V to obtain the O<sub>2</sub> concentration for each reactor position.

Figure 8 shows the O<sub>2</sub> concentrations determined by subtracting the signal of the interfering analytes. One of the graphs shows an independently measured O<sub>2</sub> concentration by exchanging H<sub>2</sub> with the non redox active gas N<sub>2</sub> on the corresponding gas inlet for comparison. All measurements show the same progression with the absolute values for each position varying randomly around an arithmetic mean, implying that the rather small variance in the obtained values is not an error introduced by the chronoamperometric subtraction algorithm but rather a real temporal difference of the local gas concentration.

**Performance Analysis and Error Discussion.** Measuring different analytes in parallel with the same sensor system in a complex setup, it is essential to investigate performance and discuss the sources of error. We analyzed key performance

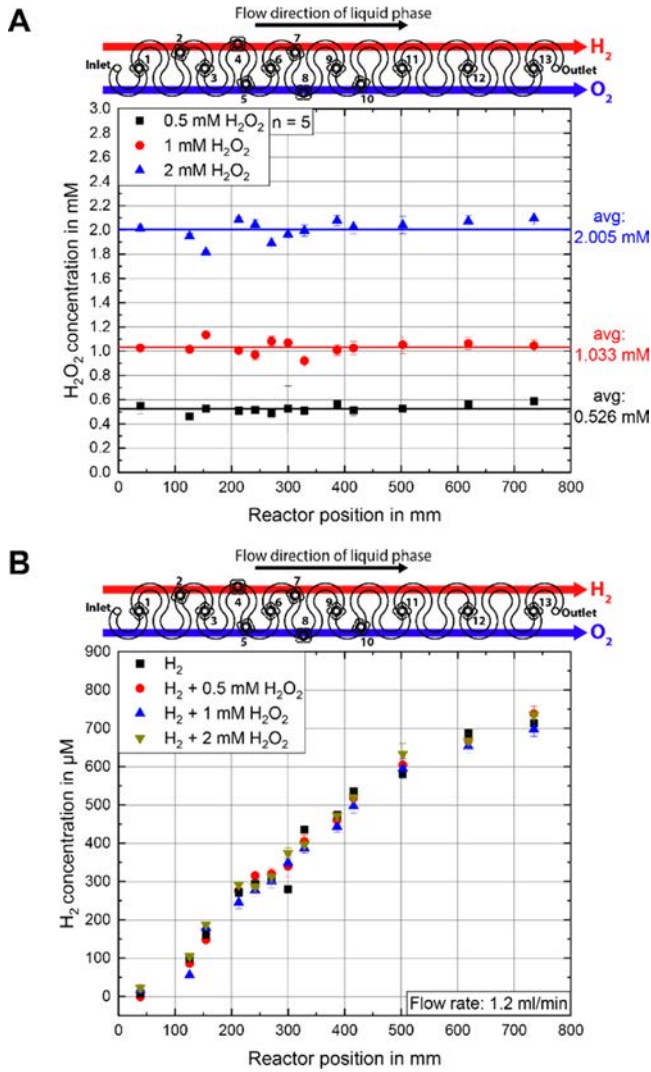


**Figure 7.** (A)  $\text{H}_2\text{O}_2$  concentrations measured along the reactor during triple analyte detection using the chronoamperometric protocol after subtraction of the  $\text{H}_2$  portion of the measurement signal at 0.95 V. The solid lines represent the average of all obtained values. (B)  $\text{H}_2$  concentrations measured along the reactor during triple analyte detection with a flow rate of 1.2 mL/min using the chronoamperometric protocol.

parameters under real measurement conditions, as summarized in Table 2. All data refer to the parallel measurement with all analytes present inside the membrane reactor using the data processing, as described previously. Thus, the deviations reflect the actual use case and include combined contributions from the sensors, method, experimental procedure, and membrane reactor.

For  $\text{H}_2\text{O}_2$ , the precision for each set of measurements (0.5–2 mM) around the mean values was between 3.2 and 4.7%. Regarding trueness, as defined by the deviation of the measured value from the values used for calibration, we determined an average absolute error between 3.2 and 6.8%. Since the absolute magnitude of the error at each measurement is roughly the same, the relative error decreases for higher concentrations. That is favorable for applications at higher concentrations. Only  $\text{H}_2$  potentially influences the  $\text{H}_2\text{O}_2$  signal. Its error additively influences the  $\text{H}_2\text{O}_2$ , but at more than one magnitude lower sensitivity, it plays a negligible role.

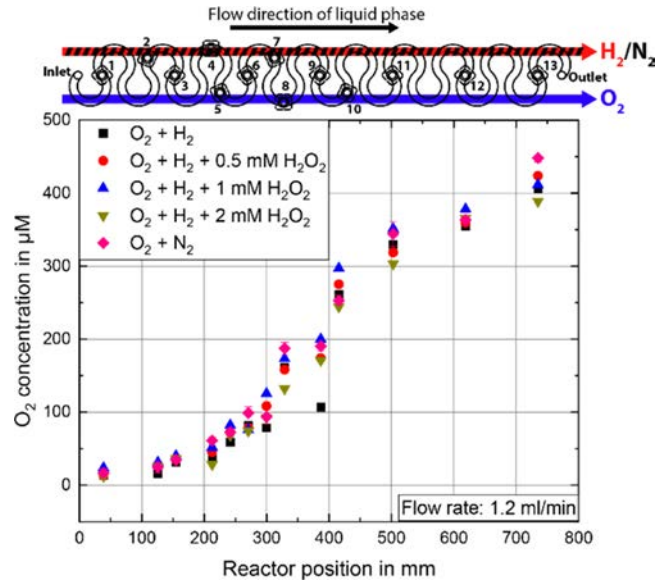


**Figure 8.**  $\text{O}_2$  concentrations measured in the reactor during triple analyte detection, using the chronoamperometric protocol, showing good agreement to the results obtained without interfering  $\text{H}_2\text{O}_2$  and  $\text{H}_2$ .

**Table 2.** Performance Parameters of the Developed Sensor Method for the Parallel Sensing of  $\text{H}_2\text{O}_2$ ,  $\text{O}_2$ , and  $\text{H}_2$  in the Actual Microreactor Application

hydrogen peroxide	relative error	remark
precision, 0.5 mM	4.7% ( $n = 13$ )	standard deviation in relation to measured mean
precision, 1 mM	3.8% ( $n = 13$ )	
precision, 2 mM	3.2% ( $n = 13$ )	
trueness, 0.5 mM	6.8% ( $n = 13$ )	mean absolute error with respect to calibration
trueness, 1 mM	4.9% ( $n = 13$ )	
trueness, 2 mM	3.2% ( $n = 13$ )	
sensitivity variation along reactor	3.6% ( $n = 13$ )	mean absolute error with respect to calibration
oxygen	relative error	remark
cross-sensitivity to $\text{H}_2\text{O}_2$	0.8% ( $n = 13$ )	mean absolute deviation after data processing
precision across all positions	14.6% ( $n = 13$ )	standard deviation, dominated by errors at low values
precision in relation to measured range	3.5% ( $n = 4 \times 13$ )	standard deviation
hydrogen	relative error	remark
cross-sensitivity to $\text{H}_2\text{O}_2$	1.2% ( $n = 13$ )	mean absolute deviation after data processing
precision across all positions	13.1% ( $n = 13$ )	standard deviation, dominated by errors at low values
precision in relation to measured range	2.6% ( $n = 4 \times 13$ )	standard deviation

$\text{H}_2\text{O}_2$  sensitivity variation along the reactor positions can be evaluated by extracting three point calibrations from the known concentrations. Along all 13 positions, sensitivity varied by 3.6%. That is in the same range as the variations in precision and trueness. Therefore, we can conclude that installing the sensors at different positions, along with opening and closing

the reactor multiple times, introduces a systematic but unavoidable variation, which seems to be a major contribution to the overall error. Sources of that error are thought to be geometrical tolerances of the sensor mounts and deviations in the distance to the membrane due to slight buckling, affecting overall mass transport by diffusion distance, position in the flow, and local disturbances of the flow.

O<sub>2</sub> and H<sub>2</sub> measurements were carried out along the reactor at different H<sub>2</sub>O<sub>2</sub> concentrations. Therefore, we can estimate the real cross sensitivity of O<sub>2</sub> and H<sub>2</sub> measurements to H<sub>2</sub>O<sub>2</sub>. Cross sensitivities for H<sub>2</sub>O<sub>2</sub> at the other two working points were determined and compared to that of O<sub>2</sub> and H<sub>2</sub>. For the O<sub>2</sub> signal, we found an average cross sensitivity to H<sub>2</sub>O<sub>2</sub> of 0.8%. For the H<sub>2</sub> signal, cross sensitivity to H<sub>2</sub>O<sub>2</sub> was 1.2%. H<sub>2</sub> is calibrated directly and selectively, so there is no influence, as expected. The O<sub>2</sub> signal depends on both H<sub>2</sub> and H<sub>2</sub>O<sub>2</sub>, where each error influences additively with roughly the same sensitivity. Since the resulting error for O<sub>2</sub> is in the same range as for H<sub>2</sub>, the subtraction works effectively. None of the cross sensitivities show a trend, and the values are lower than the scatter for H<sub>2</sub>O<sub>2</sub> measurement alone. We can therefore conclude that our developed method works very well, and highly selective signals can be obtained in practice. As mentioned before, for safety reasons, O<sub>2</sub> and H<sub>2</sub> cannot be presaturated easily in the solution at the same time. It is therefore not feasible to determine the actual cross sensitivity as described above for this case.

The different H<sub>2</sub>O<sub>2</sub> concentrations were found to have a negligible influence on O<sub>2</sub> and H<sub>2</sub> measurements. Therefore, we can also evaluate the reproducibility of the H<sub>2</sub> and O<sub>2</sub> measurements along the reactor, justifiably assuming they are independent of H<sub>2</sub>O<sub>2</sub>. The relative deviation of the O<sub>2</sub> measurements was 14.6% across all reactor positions. The relative deviation for H<sub>2</sub> was 13.1%. Both of these seemingly high relative errors are dominated by the proportionally higher errors at low concentrations. As for the H<sub>2</sub>O<sub>2</sub> measurements, these unavoidable errors come from systematic details of the setup (geometrical tolerances, assembly). The errors in relation to the full measurement range, as determined by the maximum measured concentration along the reactor, are 3.5% for O<sub>2</sub> and 2.6% for H<sub>2</sub>.

## CONCLUSIONS

We developed an electrochemical sensor protocol allowing the simultaneous, parallel determination of the concentrations for the analytes H<sub>2</sub>, O<sub>2</sub>, and H<sub>2</sub>O<sub>2</sub> on the same platinum electrode. The protocol is based on chronoamperometry. By stepping between different, thoroughly optimized, anodic and cathodic potentials in a cyclic manner, it enables us to determine the contribution of each analyte in a combined current signal and subsequently subtract the interfering signals.

The steps used in the chronoamperometric protocol were obtained by measuring each of the analytes at different potentials, spanning the whole electrochemical window of water. The final potentials were chosen according to the criteria of signal strength and overlapping signal regions. This allowed the deduction of a measurement potential for the detection of H<sub>2</sub> independent from the other two electroactive species. The nature of the interference of the individual signal contributions of each analyte for the other potential regions was tested. The results showed that each analyte signal either positively or negatively adds to the other while not influencing

each other's sensitivities. This allows the direct subtraction of the calculated signal contributions for each analyte.

The developed protocol was applied to the direct synthesis process of H<sub>2</sub>O<sub>2</sub> in membrane microreactors. For the first time, we have shown the mapping of gas distribution inside such membrane microreactors. Sensors were positioned at different locations along the reaction channel length to obtain the distribution how the analytes enter through the membrane under flow conditions. Such a measurement would not be possible with downstream techniques and shows how electrochemical sensors can deliver unique information in process engineering with the vision to control processes based on sensor data. Furthermore, the results of our in situ reactor measurement showed the validity of the applied protocol to precisely and selectively determine the concentration of the analytes H<sub>2</sub>, O<sub>2</sub>, and H<sub>2</sub>O<sub>2</sub> by the same electrode when all are present in the same electrolyte. In previous works, we have shown measurement of these analytes at high pressures. For the resulting high concentrations, it has yet to be shown how far the superposition of the currents behaves in a linear additive manner. Nonetheless, we have shown that the presented method can provide a potent way of determining concentrations of multianalyte systems. The overall approach is not limited to the application case or analytes shown in this work and could be applied to, for example, different reactive oxygen/nitrogen species or neurotransmitters.

## AUTHOR INFORMATION

### Corresponding Author

**Andreas Weltin** – Laboratory for Sensors,  
IMTEK–Department of Microsystems Engineering,  
University of Freiburg, 79110 Freiburg, Germany;  
orcid.org/0000 0001 8288 8266; Phone: +49 761 203  
7263; Email: weltin@imtek.de

### Authors

**Sebastian Urban** – Laboratory for Sensors,  
IMTEK–Department of Microsystems Engineering,  
University of Freiburg, 79110 Freiburg, Germany;  
orcid.org/0000 0002 0107 4242

**Benedikt J. Deschner** – Institute for Micro Process  
Engineering (IMVT), Karlsruhe Institute of Technology,  
76344 Eggenstein Leopoldshafen, Germany; orcid.org/  
0000 0001 5800 7510

**Laura L. Trinkies** – Institute for Micro Process Engineering  
(IMVT), Karlsruhe Institute of Technology, 76344  
Eggenstein Leopoldshafen, Germany

**Jochen Kieninger** – Laboratory for Sensors,  
IMTEK–Department of Microsystems Engineering,  
University of Freiburg, 79110 Freiburg, Germany;  
orcid.org/0000 0001 8220 8814

**Manfred Kraut** – Institute for Micro Process Engineering  
(IMVT), Karlsruhe Institute of Technology, 76344  
Eggenstein Leopoldshafen, Germany

**Roland Dittmeyer** – Institute for Micro Process Engineering  
(IMVT), Karlsruhe Institute of Technology, 76344  
Eggenstein Leopoldshafen, Germany; orcid.org/0000  
0002 3110 6989

**Gerald A. Urban** – Laboratory for Sensors,  
IMTEK–Department of Microsystems Engineering,  
University of Freiburg, 79110 Freiburg, Germany

## Notes

The authors declare no competing financial interest.

## ACKNOWLEDGMENTS

Financial support by the German Research Foundation (DFG) through Research Unit FOR 2383, “ProMiSe” (www.promise.kit.edu), under grant nos. Di 696/13 1, Di 696/13 2, UR 70/11 1, and UR 70/11 2 is gratefully acknowledged.

## REFERENCES

- (1) Hanrahan, G.; Patil, D. G.; Wang, J. Electrochemical Sensors for Environmental Monitoring: Design, Development and Applications. *J. Environ. Monit.* **2004**, *6*, 657–664.
- (2) Bakker, E.; Telting Diaz, M. Electrochemical Sensors. *Anal. Chem.* **2002**, *74*, 2781–2800.
- (3) Privett, B. J.; Shin, J. H.; Schoenfish, M. H. Electrochemical Sensors. *Anal. Chem.* **2008**, *80*, 4499–4517.
- (4) Yang, T.; Yu, R.; Yan, Y.; Zeng, H.; Luo, S.; Liu, N.; Morrin, A.; Luo, X.; Li, W. A Review of Ratiometric Electrochemical Sensors: From Design Schemes to Future Prospects. *Sens. Actuators, B* **2018**, *274*, 501–516.
- (5) Kieninger, J.; Weltin, A.; Flamm, H.; Urban, G. A. Microsensor Systems for Cell Metabolism from 2D Culture to Organ on Chip. *Lab Chip* **2018**, *18*, 1274–1291.
- (6) Weltin, A.; Kieninger, J.; Urban, G. A. Microfabricated, Amperometric, Enzyme Based Biosensors for in Vivo Applications. *Anal. Bioanal. Chem.* **2016**, *408*, 4503–4521.
- (7) Labib, M.; Sargent, E. H.; Kelley, S. O. Electrochemical Methods for the Analysis of Clinically Relevant Biomolecules. *Chem. Rev.* **2016**, *116*, 9001–9090.
- (8) Batley, G. E. Electroanalytical Techniques for the Determination of Heavy Metals in Seawater. *Mar. Chem.* **1983**, *12*, 107–117.
- (9) Wang, J. In Situ Electrochemical Monitoring: From Remote Sensors to Submersible Microlaboratories. *Lab. Rob. Autom.* **2000**, *12*, 178–182.
- (10) Howell, K. A.; Achterberg, E. P.; Braungardt, C. B.; Tappin, A. D.; Turner, D. R.; Worsfold, P. J. The Determination of Trace Metals in Estuarine and Coastal Waters Using a Voltammetric in Situ Profiling System. *Analyst* **2003**, *128*, 734–741.
- (11) Tercier, M. L.; Buffle, J. In Situ Voltammetric Measurements in Natural Waters: Future Prospects and Challenges. *Electroanalysis* **1993**, *5*, 187–200.
- (12) Barek, J.; Cvačka, J.; Muck, A.; Quaiserová, V.; Zima, J. Electrochemical Methods for Monitoring of Environmental Carcinogens. *Anal. Bioanal. Chem.* **2001**, *369*, 556–562.
- (13) Liebisch, F.; Weltin, A.; Marzioch, J.; Urban, G. A.; Kieninger, J. Zero Consumption Clark Type Microsensor for Oxygen Monitoring in Cell Culture and Organ on Chip Systems. *Sens. Actuators, B* **2020**, *322*, 128652.
- (14) Mir, M.; Homs, A.; Samitier, J. Integrated Electrochemical DNA Biosensors for Lab on a Chip Devices. *Electrophoresis* **2009**, *30*, 3386–3397.
- (15) Simoska, O.; Stevenson, K. J. Electrochemical Sensors for Rapid Diagnosis of Pathogens in Real Time. *Analyst* **2019**, *144*, 6461–6478.
- (16) Fernández la Villa, A.; Pozo Ayuso, D. F.; Castaño Álvarez, M. Microfluidics and Electrochemistry: An Emerging Tandem for next Generation Analytical Microsystems. *Curr. Opin. Electrochem.* **2019**, *15*, 175–185.
- (17) Odijk, M.; Van Den Berg, A. Nanoscale Electrochemical Sensing and Processing in Microreactors. *Annu. Rev. Anal. Chem.* **2018**, *11*, 421–440.
- (18) Lozeman, J. J. A.; Elsbecker, T.; Bohnenn, S.; De Boer, H. L.; Krakkers, M.; Mul, G.; Van Den Berg, A.; Odijk, M. Modular Microreactor with Integrated Reflection Element for Online Reaction Monitoring Using Infrared Spectroscopy. *Lab Chip* **2020**, *20*, 4166–4174.
- (19) Ciriminna, R.; Albanese, L.; Meneguzzo, F.; Pagliaro, M. Hydrogen Peroxide: A Key Chemical for Today’s Sustainable Development. *ChemSusChem* **2016**, *9*, 3374–3381.
- (20) Melchionna, M.; Fornasiero, P.; Prato, M. The Rise of Hydrogen Peroxide as the Main Product by Metal Free Catalysis in Oxygen Reductions. *Adv. Mater.* **2019**, *31*, 1802920.
- (21) García Serna, J.; Moreno, T.; Biasi, P.; Cocero, M. J.; Mikkola, J. P.; Salmi, T. O. Engineering in Direct Synthesis of Hydrogen Peroxide: Targets, Reactors and Guidelines for Operational Conditions. *Green Chem.* **2014**, *16*, 2320.
- (22) Campos Martin, J. M.; Blanco Brieva, G.; Fierro, J. L. G. Hydrogen Peroxide Synthesis: An Outlook beyond the Anthraquinone Process. *Angew. Chem., Int. Ed.* **2006**, *45*, 6962–6984.
- (23) Pennemann, H.; Kolb, G. Review: Microstructured Reactors as Efficient Tool for the Operation of Selective Oxidation Reactions. *Catal. Today* **2016**, *278*, 3–21.
- (24) Riedl, H. J.; Pfeleiderer, G. Production of Hydrogen Peroxide. U.S. Patent 2,158,525 A, 1939.
- (25) Edwards, J. K.; Freakley, S. J.; Lewis, R. J.; Pritchard, J. C.; Hutchings, G. J. Advances in the Direct Synthesis of Hydrogen Peroxide from Hydrogen and Oxygen. *Catal. Today* **2015**, *248*, 3–9.
- (26) Iglesias, D.; Giuliani, A.; Melchionna, M.; Marchesan, S.; Criado, A.; Nasi, L.; Bevilacqua, M.; Tavagnacco, C.; Vizza, F.; Prato, M.; Fornasiero, P. N Doped Graphitized Carbon Nanohorns as a Forefront Electrocatalyst in Highly Selective O<sub>2</sub> Reduction to H<sub>2</sub>O<sub>2</sub>. *Chem* **2018**, *4*, 106–123.
- (27) Yang, S.; Verdaguer Casadevall, A.; Arnarson, L.; Silvioni, L.; Colic, V.; Frydendal, R.; Rossmeisl, J.; Chorkendorff, I.; Stephens, I. E. L. Towards the Decentralized Electrochemical Production of H<sub>2</sub>O<sub>2</sub>: A Focus on the Catalysis. *Sustainable Environ. Res.* **2018**, *8*, 4064–4081.
- (28) Chen, Z.; Chen, S.; Siahrostami, S.; Chakhranont, P.; Hahn, C.; Nordlund, D.; Dimosthenis, S.; Nørskov, J. K.; Bao, Z.; Jaramillo, T. F. Development of a Reactor with Carbon Catalysts for Modular Scale, Low Cost Electrochemical Generation of H<sub>2</sub>O<sub>2</sub>. *React. Chem. Eng.* **2017**, *2*, 239–245.
- (29) Centi, G.; Perathoner, S.; Abate, S. Direct Synthesis of Hydrogen Peroxide: Recent Advances. *Modern Heterogeneous Oxidation Catalysis*; Wiley VCH Verlag, 2009; pp 253–287.
- (30) Dittmeyer, R.; Grunwaldt, J. D.; Pashkova, A. A Review of Catalyst Performance and Novel Reaction Engineering Concepts in Direct Synthesis of Hydrogen Peroxide. *Catal. Today* **2015**, *248*, 149–159.
- (31) Selinsek, M.; Bohrer, M.; Vankayala, B. K.; Haas Santo, K.; Kraut, M.; Dittmeyer, R. Towards a New Membrane Micro Reactor System for Direct Synthesis of Hydrogen Peroxide. *Catal. Today* **2016**, *268*, 85–94.
- (32) Selinsek, M.; Kraut, M.; Dittmeyer, R. Experimental Evaluation of a Membrane Micro Channel Reactor for Liquid Phase Direct Synthesis of Hydrogen Peroxide in Continuous Flow Using Nafion Membranes for Safe Utilization of Undiluted Reactants. *Catalysts* **2018**, *8*, 556.
- (33) Gallina, G.; García Serna, J.; Salmi, T. O.; Canu, P.; Biasi, P. Bromide and Acids: A Comprehensive Study on Their Role on the Hydrogen Peroxide Direct Synthesis. *Ind. Eng. Chem. Res.* **2017**, *56*, 13367.
- (34) Inoue, T.; Ohtaki, K.; Murakami, S.; Matsumoto, S. Direct Synthesis of Hydrogen Peroxide Based on Microreactor Technology. *Fuel Process. Technol.* **2013**, *108*, 8–11.
- (35) Hu, A. L.; Liu, Y. H.; Deng, H. H.; Hong, G. L.; Liu, A. L.; Lin, X. H.; Xia, X. H.; Chen, W. Fluorescent Hydrogen Peroxide Sensor Based on Cupric Oxide Nanoparticles and Its Application for Glucose and L Lactate Detection. *Biosens. Bioelectron.* **2014**, *61*, 374–378.
- (36) Tsaplev, Y. B. Chemiluminescence Determination of Hydrogen Peroxide. *J. Anal. Chem.* **2012**, *67*, 506–514.
- (37) Hu, Y.; Zhang, Z.; Yang, C. The Determination of Hydrogen Peroxide Generated from Cigarette Smoke with an Ultrasensitive and Highly Selective Chemiluminescence Method. *Anal. Chim. Acta* **2007**, *601*, 95–100.

- (38) Khorami, H. A.; Botero Cadavid, J. F.; Wild, P.; Djilali, N. Spectroscopic Detection of Hydrogen Peroxide with an Optical Fiber Probe Using Chemically Deposited Prussian Blue. *Electrochim. Acta* **2014**, *115*, 416–424.
- (39) Urban, S.; Weltin, A.; Flamm, H.; Kieninger, J.; Deschner, B. J.; Kraut, M.; Dittmeyer, R.; Urban, G. A. Electrochemical Multisensor System for Monitoring Hydrogen Peroxide, Hydrogen and Oxygen in Direct Synthesis Microreactors. *Sens. Actuators, B* **2018**, *273*, 973–982.
- (40) Urban, S.; Tamilselvi Sundaram, V.; Kieninger, J.; Urban, G.; Weltin, A. Microsensor Electrodes for 3D Inline Process Monitoring in Multiphase Microreactors. *Sensors* **2020**, *20*, 4876.
- (41) Solvay. Passivation Procedure. [https://www.solvay.us/en/binaries/HH\\_056\\_Passivation\\_236794.pdf](https://www.solvay.us/en/binaries/HH_056_Passivation_236794.pdf) (accessed Oct 28, 2020).
- (42) Schröder, V.; Emonts, B.; Janßen, H.; Schulze, H. P. Explosion Limits of Hydrogen/Oxygen Mixtures at Initial Pressures up to 200 Bar. *Chem. Eng. Technol.* **2004**, *27*, 847–851.
- (43) Weltin, A.; Kieninger, J.; Enderle, B.; Gellner, A. K.; Fritsch, B.; Urban, G. A. Polymer Based, Flexible Glutamate and Lactate Microsensors for in Vivo Applications. *Biosens. Bioelectron.* **2014**, *61*, 192–199.
- (44) Bao, J.; Macdonald, D. D. Oxidation of Hydrogen on Oxidized Platinum. Part I: The Tunneling Current. *J. Electroanal. Chem.* **2007**, *600*, 205–216.
- (45) Hang Li, Y.; Xing, J.; Jia Chen, Z.; Li, Z.; Tian, F.; Rong Zheng, L.; Feng Wang, H.; Hu, P.; Jun Zhao, H.; Gui Yang, H. Unidirectional Suppression of Hydrogen Oxidation on Oxidized Platinum Clusters. *Nat. Commun.* **2013**, *4*, 1–7.
- (46) Hall, S. B.; Khudaish, E. A.; Hart, A. L. Electrochemical Oxidation of Hydrogen Peroxide at Platinum Electrodes. Part 1. An Adsorption Controlled Mechanism. *Electrochim. Acta* **1998**, *43*, 579–588.
- (47) Bagotzky, V. S.; Vassilyev, Y. B.; Weber, J.; Pirtskhalava, J. N. Adsorption of Anions on Smooth Platinum Electrodes. *J. Electroanal. Chem.* **1970**, *27*, 31–46.
- (48) Xu, J.; Georgescu, N. S.; Scherson, D. A. The Oxidation of Bromide on Platinum Electrodes in Aqueous Acidic Solutions: Electrochemical and In Situ Spectroscopic Studies. *J. Electrochem. Soc.* **2014**, *161*, H392–H398.
- (49) Rodney, A. N.; Karp, S. Non Additive Voltammetric Limiting Currents of Acrylamide with Oxygen and Hydrogen Peroxide. *J. Electroanal. Chem.* **2014**, *714–715*, 76–78.
- (50) Dass, A.; Leventis, N. Non Additive Voltammetric Currents from Multicomponent Systems of Redox Active Substances. *Electrochim. Acta* **2005**, *50*, 4134–4139.
- (51) Miller, S. L.; Orlemann, E. F. Non Additivity of Polarographic Diffusion Currents with Mixtures of Certain Reducible Species. *J. Am. Chem. Soc.* **1953**, *75*, 2001–2003.
- (52) Urban, S.; Kieninger, J.; Deschner, B. J.; Kraut, M.; Dittmeyer, R.; Urban, G. A.; Weltin, A. Multiparametric, Spatially Resolved Detection of H<sub>2</sub>O<sub>2</sub> and O<sub>2</sub> with Electrochemical Microsensor Array in Synthesis Membrane Microreactors. *2019 20th International Conference on Solid State Sensors, Actuators Microsystems Eurosensors XXXIII, TRANSDUCERS 2019 EUROSensors XXXIII*, 2019; 1297–1300.
- (53) Weltin, A.; Ganatra, D.; König, K.; Joseph, K.; Hofmann, U. G.; Urban, G. A.; Kieninger, J. New Life for Old Wires: Electrochemical Sensor Method for Neural Implants. *J. Neural. Eng.* **2020**, *17*, 016007.
- (54) *CRC Handbook of Chemistry and Physics*; Lide, D. R.; Baysinger, G.; Berger, L. I.; Goldberg, R. N.; Kehiaian, H. V.; Kuchitsu, K.; Rosenblatt, G.; Roth, D. L.; Zwillinger, D.; CRC Press, 2004.

## Repository KITopen

Dies ist ein Postprint/begutachtetes Manuskript.

Empfohlene Zitierung:

Urban, S.; Deschner, B. J.; Trinkies, L. L.; Kieninger, J.; Kraut, M.; Dittmeyer, R.; Urban, G. A.; Weltin, A.

[In Situ Mapping of H<sub>2</sub>, O<sub>2</sub>, and H<sub>2</sub>O<sub>2</sub> in Microreactors : A Parallel, Selective Multianalyte Detection Method.](#)

2021. ACS sensors, 6

[doi: 10.544/IR/1000135102](#)

Zitierung der Originalveröffentlichung:

Urban, S.; Deschner, B. J.; Trinkies, L. L.; Kieninger, J.; Kraut, M.; Dittmeyer, R.; Urban, G. A.; Weltin, A.

[In Situ Mapping of H<sub>2</sub>, O<sub>2</sub>, and H<sub>2</sub>O<sub>2</sub> in Microreactors : A Parallel, Selective Multianalyte Detection Method.](#)

2021. ACS sensors, 6 (4), 1583–1594

[doi:10.1021/acssensors.0c02509](#)

Lizenzinformationen: [KITopen-Lizenz](#)